Size-induced acoustic hardening and optic softening of phonons in InP, CeO$_2$, SnO$_2$, CdS, Ag, and Si nanostructures

Chang Q. Sun,[1,*] L. K. Pan,[1] C. M. Li,[1] and S. Li[2]

[1]*School of Electrical and Electronic Engineering Nanyang Technological University, Singapore 639798*
[2]*School of Materials Science and Engineering, the University of New South Wales, Sydney NSW 2052, Australia*

It has long been a puzzle that the Raman optical modes shift to lower frequency (or termed optical mode softening or redshift) associated with the creation of Raman acoustic modes that shift to higher energy (or called acoustic hardening or blueshift) upon a nanosolid being formed and its size being reduced. Understandings of the mechanism behind the size-induced Raman shifts have been quite controversial. On the basis of the bond-order–length–strength (BOLS) correlation mechanism [Phys. Rev. B **69**, 045105 (2004)], we show that the optical softening arises from atomic cohesive energy weakening of atoms in the surface skins, whereas the acoustic mode hardening is predominated by intergrain interactions. Agreement between predictions and observations has been realized for Ag, Si, CdS, InP, TiO$_2$, CeO$_2$, and SnO$_2$ nanostructures with elucidation of vibration frequencies of the corresponding isolated dimers from fitting the optical softening.

I. INTRODUCTION

Atomic vibration is of high interest because the behavior of phonons influences directly the electrical and optical properties in solid materials and devices.[1] For instance, electron-phonon couplings play a significant role in photoabsorption and photoemission. Phonon scattering forms an important component in thermal and electrical transport dynamics. It has long been surprising that with structural miniaturization down to nanometer scale the optical Raman modes shift down to lower frequency[2] (or called optical mode softening) accompanied by the generation of low-frequency Raman (LFR) acoustic modes at wave numbers of a few or a few tens cm^{-1}. The LFR peak shifts up (or called acoustic mode hardening) towards higher frequency upon the solid size being reduced.[3,4] Generally, the size-dependent Raman shifts follow a scaling relation[2,4]

$$\omega(K_j) - \omega(\infty) = A_f/K_j^\kappa,$$

where A_f and κ are adjustable parameters for data fitting. K_j, the dimensionless form of size, is the number of atoms with diameter d lined along the radius (R_j) of a spherical dot. For optical redshift, $A_f < 0$; for the LFR acoustic blueshift, $A_f > 0$. The index κ varies from 1.0 to 2.0, depending on the mode of vibration and varying from source to source.[5] For the Si optical mode $\kappa = 1.08$–2.0, $\omega(\infty) = 520$ cm^{-1} corresponds to a wavelength of 2×10^4 nm. The LFR mode disappears for large particles because $\omega(\infty) = 0$.

The underlying mechanism behind the Raman shift is under debate with numerous theories. Theoretical studies of the Raman shift are often based on a continuum dielectric mechanism.[6,7] Sophisticated calculations have been carried out using models of the correlation length,[8] bulk phonon dispersion,[9] and lattice-dynamic matrix,[10,11] associated with the microscopic valence force field,[4] phonon confinement,[12] and bond polarization mechanism.[2]

The mechanism of quadrupolar vibration taking the individual nanoparticle as a whole was assumed to be responsible for the LFR acoustic modes. The phonon energies are size dependent and vary with the materials of the host matrix. The LFR scattering from silver nanoclusters embedded in porous alumina (Ref. 13) and SiO$_2$ (Ref. 14) was suggested to arise from the quadrupolar vibration modes that are enhanced by the excitation of the surface plasmas of the encapsulated Ag particles. The selection of modes by LFR scattering is suggested to arise from the stronger plasmon-phonon coupling for these modes. For an Ag particle smaller than 4 nm, the size dependence of the frequency peak can be explained using Lamb's theory,[15] which gives vibrational frequencies of a homogeneous elastic body with a spherical form. Zi, Zhang, and Xie[11] calculated the Raman scattering from acoustic phonons in Si nanocrystals by a lattice-dynamical model.[10] The polarized and depolarized low-frequency Raman peaks were ascribed as confined LA-like and TA-like acoustic phonons, respectively. They found that the effects of the matrix are important, which will lead to a redshift for both polarized and depolarized Raman peaks. Their approaches improve the fit to the measurement compared with calculations using Lamb's model.[15] On the other hand, lattice strain was suggested to be another possible mechanism for the LFR blueshift as size-dependent compressive strain is present as has been observed from CdS$_x$Se$_{1-x}$ nanocrystals embedded in a borosilicate (B$_2$O$_3$−SiO$_2$) glass matrix.[16] It was explained that the lattice strain enhances the surface stress when the crystal size is reduced. The observed blueshift of acoustic phonon energies was suggested to be a consequence of the compressive stress that overcomes the redshift caused by phonon confinement. Liang *et al.*[17] have proposed a model for the Raman blueshift by relating the frequency shift to the bond length and bond strength, which are functions of the entropy, latent heat of fusion, and critical temperature for solid-liquid transitions.

The redshifts of optical modes have been suggested to be activated by surface disorder,[18] surface stress,[19,20] and phonon quantum confinement,[21,22] as well as surface chemical passivation.[23] The phonon confinement model attributes the

redshift of the Raman line to the relaxation of the wave-vector selection rule ($\Delta q = 0$) for the excitation of the Raman-active phonons due to their localization. The relaxation of the selection rule arises from the finite crystalline size and the diameter distribution of nanosolid in the films. When the size is decreased, the rule of momentum conservation will be relaxed and the Raman-active modes will not be limited at the center of the Brillouin zone.[19] A Gaussian-type phonon confinement model[22] indicates that strong phonon damping is present whereas calculations[24] using the correlation functions of the local dielectric constant ignore the role of phonon damping in the nanosolid. The large surface-to-volume ratio of a nanodot strongly affects the optical properties because of the introduction of surface polarization and surface states.[25] Using a phenomenological Gaussian envelope function of phonon amplitudes, Tanaka *et al.*[26] showed that the size dependence of the optic redshift originated from the relaxation of the $\Delta q = 0$ selection rule based on the phonon confinement argument with negative phonon dispersion. The phonon energies for all the glasses are reduced, and the values of the phonon energies of CdSe nanodots are found to be quite different for various glass host matrices. A sophisticated analytical model of Hwang *et al.*[5] indicates that the effect of lattice strain must be considered in explaining the optical redshift for CdSe nanodots embedded in different glass matrices. For a free surface, it has been derived that the redshift follows the relation

$$\frac{\Delta\omega(K_j)}{\omega(\infty)} = BK_j^{-2}. \tag{1}$$

The value of B in Eq. (1) is a competition between the phonon negative dispersion and the size-dependent surface tension. Thus, a positive value of B indicates that the phonon negative dispersion exceeds the size-dependent surface tension and consequently causes the redshift of phonon frequency and vice versa. In case of a balance of the two effects—i.e., $B = 0$—the size dependence disappears. However, there are still some difficulties in using this equation because of some uncertainties of the parameters involved, as remarked on by Hwang *et al.*[5]

It is noted that currently available models for the optical redshift are based on assumptions that the materials are homogeneous and isotropic, which is valid only in the long-wavelength limit. When the size of the nanosolid is in the range of a few nanometers the continuum dielectric models exhibit limitations. Therefore, the models discussed could hardly reproduce with satisfactory the Raman frequency shifts, in particular at the lower end of the size limit. Furthermore, it is yet unclear how the quantum confinement and surface strain dictate the Raman shift of both the optical and acoustic modes. The objective of this work is to show that derivatives of the recent bond-order–length–strength (BOLS) correlation mechanism[27–29] could reproduce the size-induced Raman shifts, leading to a deeper and consistent insight into the mechanism behind with elucidation of the vibration frequency of the corresponding dimers, which is beyond the scope of other sophisticated models.

II. PRINCIPLE

A. Vibration modes

Raman scattering is known to arise from the radiating dipole moment induced in a system by the electric field of incident electromagnetic radiation. The laws of momentum and energy conservation govern the interaction between a phonon and the incident photon. When we consider a solid containing numerous Bravais unit cells and each cell contains n atoms, there will be $3n$ modes of vibrations. Among the $3n$ modes there will be three acoustic modes, LA, TA$_1$, and TA$_2$ and $3(n-1)$ optical modes LO and TO. The acoustic modes represent the in-phase motion of the mass center of the unit cell or the entire solid as a whole. The long-range Coulomb interaction is responsible for the intercluster interaction. Therefore, the acoustic LFR mode should arise from the vibration of the entire nanosolid interacting with the host matrix or with other neighboring clusters. Therefore, it is expected that the LTR mode approaches zero if the particle size is infinitely large, as one can observe. The optical modes arise from the relative motion of the individual atoms in a complex unit cell. For elemental solids with a simple crystal structure such as the fcc of Ag, only acoustic modes present. Silicon or diamond is an interlock of two fcc unit cells that contain in each cell two atoms in nonequivalent positions; there will be three acoustic modes and three optical modes.

B. Size-dependent optical frequency shift

1. BOLS correlation

The BOLS correlation mechanism[27–30] relates the size dependence of nanostructures to the effect of bond order loss on the interatomic bonding and its consequence on binding energy density per unit volume and the cohesive energy per discrete atom in the nanostructures. Involvement of interatomic interactions differentiates the performance of a solid from that of an isolated atom, and the variation of the portion of surface atoms could tune the nanosolid properties in many aspects. The BOLS correlation mechanism indicates that the bond order loss of a surface atom causes the remaining bonds of the lower-coordinated atoms to contract spontaneously ($d_i = c_i d$) associated with bond strength gain or atomic trapping potential well suppression ($E_i = c_i^{-m} E_b$), where d is the bond length and E_i is the single bond energy. The subscript i and b denotes atoms in a specific ith atomic layer and the bulk one, respectively. The i is counted from the outermost atomic layer to the center of the solid. The bond contraction coefficient $c_i = 2/\{1 + \exp[(12 - z_i)/(8z_i)]\}$ is a function of atomic coordination, which fits ideally the correlation of bond-order–bond-length of Goldschmidt, Pauling, and Feibelman.[31] The index m recognizes the nature of the bond involved.

As consequences of the BOLS correlation, densification happens to the charge, mass, and energy in the relaxed region. Energy density enhancement contributes to the crystal potential and hence the Hamiltonian of an electron (the sum of the kinetic energy, intra-atomic trapping potential, and interatomic potential energy for the specific electron) in the solid and the associated properties such as the band and

band-gap widths, core-level shift, Stokes shift (electron-phonon interaction), and dielectric suppression. On the other hand, the competition between bond-order loss and the associated bond-strength gain contributes to the atomic cohesive energy (the sum of bond energy over all the coordinates of an atom) that dictates the thermal and mechanical properties of the solid such as phase stability, self-assembly growth, and activation energy for atomic vibration, diffusion, and dislocation in a solid. Refer to Refs. 27–30 (and references therein) for a detailed description of the BOLS correlation and its applications.

2. Lattice vibration frequency

The total energy E causing lattice vibration consists of the component of short-range interactions E_S and the component of long-range Coulomb interactions E_C (Ref. 4):

$$E = E_S + E_C. \tag{2}$$

The long-range part corresponds to the LFR mode and represents the weak interaction between nanosolids. The short-range energy E_S arises from the nearest bonding atoms, which is composed of two parts. One is the lattice thermal vibration $E_V(T)$ and the other is the interatomic binding energy at 0 K, $E_b(r)$. The E_S for a dimer can be expressed as a Taylor's series[27]

$$E_S(r,T) = \sum_{n \geqslant 0} \left(\frac{d^n u(r)}{n!\, dr^n} \right)_{r=d} (r-d)^n = u(d) + 0$$

$$+ \left. \frac{d^2 u(r)}{2!\, dr^2} \right|_d (r-d)^2 + \left. \frac{d^3 u(r)}{3!\, dr^3} \right|_d (r-d)^3$$

$$= E_b(d) + E_V(T). \tag{3}$$

The term with index $n=0$ corresponds to the minimal binding energy at $T=0$ K, and $u(d)=E_b(d)<0$ is the binding energy at $T=0$ K. The term $n=1$ is the force $[\partial u(r)/\partial r|_d=0]$ at equilibrium, and the terms with $n \geqslant 2$ correspond to the thermal vibration energy $E_V(T)$. By definition, the thermal vibration energy of a single bond is approximated as[32]

$$E_V(T) = \left. \frac{d^2 u(r)}{2!\, dr^2} \right|_d (r-d)^2 + \left. \frac{d^3 u(r)}{3!\, dr^3} \right|_d (r-d)^3$$

$$\cong \mu \omega^2 (r-d)^2/2 + 0[(r-d)^{n>2}] \approx k_v (r-d)^2/2, \tag{4}$$

where $r-d=x$ is the magnitude of lattice vibration, which reaches a maximum of 3% of the bond length at the temperature of melting.[32] μ is the reduced mass of the dimer of concern. Here $k_v = \mu \omega^2 \propto E_b/d^2$ is the force constant for lattice vibration with an angular frequency of ω. The high-order contribution (for $n>2$) is negligibly small if the temperature of the measurement is not sufficiently high such as near the melting point.

For a single bond, the k_v is strengthened because of the bond-order-loss-induced bond contraction and bond strength gain.[27–30] For a single atom, we have to count the contributions from all neighboring bonds. For a lower-coordinated atom the resultant k_v could be lower because of the bond

order loss. Considering the vibration amplitude $x \ll d$, it is convenient and reasonable to take the mean contribution from each coordinate to the force constant and to the magnitude of dislocation as the first-order approximation:

$$k_1 = k_2 = \ldots = k_z = \mu_i \omega^2$$

and

$$x_1 = x_2 = \ldots = x_z = (r-d)/z.$$

Therefore the total energy of a certain atom with z coordinates is the sum over all coordinates,

$$E_S(d,T) = \sum_z \left[E_b + \frac{\mu \omega^2}{2} \left(\frac{r-d}{z} \right)^2 + \cdots \right]$$

$$= zE_b + \left. \frac{z d^2 u(r)}{2!\, dr^2} \right|_d (r-d)^2 + \cdots. \tag{5}$$

This relation leads to an expression for the phonon frequency as a function of bond energy and atomic CN, and bond length,

$$\omega = z \left[\left. \frac{d^2 u(r)}{\mu dr^2} \right|_d \right]^{1/2} \propto \frac{z E_b^{1/2}}{d}. \tag{6}$$

3. Size dependence

A physically detectable quantity that depends on the atomic cohesive energy or the Hamiltonian for a nanosolid can be expressed as $Q(K_j)$ in a shell structure:

$$Q(K_j) = Nq_0 + \sum_{i \leqslant 3} N_i (q_i - q_0),$$

$$\frac{Q(K_j) - Q(\infty)}{Q(\infty)} = \sum_{i \leqslant 3} \gamma_{ij} \frac{\Delta q_i}{q_0},$$

where

$$\gamma_{ij} = \frac{N_i}{N} = \frac{V_i}{V} \approx \begin{cases} 1, & K_j \leqslant 3, \\ \dfrac{\tau c_i}{K_j}, & \text{otherwise,} \end{cases} \tag{7}$$

where $Q(\infty)=Nq_0$ is for a bulk solid. q_0 and q_S correspond to the Q value per atomic volume inside the bulk and in the surface region, respectively. γ_i is the portion of atoms in the ith atomic layer over the total number of atoms of the entire solid of different shapes ($\tau=1$, 2, 3 correspond to a thin plate, a rod, and a spherical dot, respectively). Combining Eqs. (6) and (7) gives the size-dependent optic redshift [where $Q(\infty)=\omega(\infty)-\omega(1)$]

$$\frac{\omega(K_j) - \omega(\infty)}{\omega(\infty) - \omega(1)} = \sum_{i \leqslant 3} \gamma_i \left[\frac{\omega_i}{\omega_b} - 1 \right]$$

$$= \sum_{i \leqslant 3} \gamma_i \left[\frac{z_i}{z_b} c_i^{-(m/2+1)} - 1 \right] = \Delta_p < 0,$$

where

$$z_1 = 4(1 - 0.75/K_f) \quad \text{(spherical)},$$
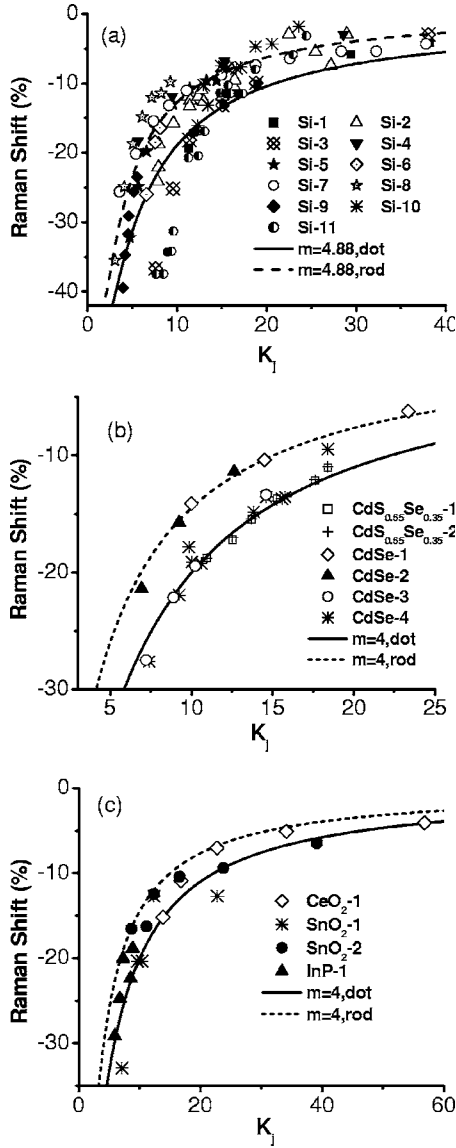
FIG. 1. Comparison of the BOLS predictions (lines for different shapes) with theoretical and experimental observations (scattered data) on the size-dependent optic phonon softening of a nanosolid. (a) Data labeled Si-1 were calculated using the correlation length model (Ref. 8), Si-3 (dot) and Si-4 (rod) were calculated using the bulk dispersion relation of phonons (Ref. 9), Si-5 was calculated from the lattice-dynamic matrix (Ref. 4), Si-7 was calculated using phonon confinement model (Ref. 12), and Si-8 (rod) and Si-9 (dot) were calculated using bond polarizability model (Ref. 2). Data for Si-2 (Ref. 35), Si-6 (Ref. 36), and Si-10 and Si-11 (Ref. 19) are measured data. (b) $CdS_{0.65}Se_{0.35}$-1, $CdS_{0.65}Se_{0.35}$ (in glass)-LO_2, $CdS_{0.65}Se_{0.35}$-2, $CdS_{0.65}Se_{0.35}$ (in glass)-LO_1 (Ref. 37), CdSe-1, CdSe(in $B_2O_3SiO_2$)-LO, CdSe-2, CdSe(in SiO_2)-LO, and CdSe-3 CdSe(in GeO_2)-LO, CdSe-4, CdSe(in GeO_2)-LO (Ref. 26), (c) CeO_2-1 (Ref. 38), SnO_2-1 (Ref. 39), SnO_2-2 (Ref. 18), and InP (Ref. 40) are all measurements.

$$z_2 = 6, \quad z_3 = 12. \tag{8}$$

$\omega(1)$ is the vibrational frequency of an isolated dimer, which is the reference point for the optical redshift upon nanosolid and bulk formation. The index i is counted up to 3 from the outmost atomic layer to the center of the solid as no atomic CN imperfection is justified at $i > 3$.

III. RESULTS AND DISCUSSION

A. Optical modes and dimer vibration

In experiment, one can only measure $\omega(\infty)$ and $\omega(K_j)$ in Eq. (8). However, with the known m value derived from the measurement of other quantities such as the melting point or core-level energy,[27–30] one can determine $\omega(1)$ or the bulk shift $\omega(\infty) - \omega(1)$ by matching the measured data of the size dependence data to the theoretical predicted line:

$$\Delta\omega(K_j) = \begin{cases} \dfrac{-A'}{K_j^\kappa} & \text{(measurement)}, \\ \Delta_R[\omega(\infty) - \omega(1)] & \text{(theory)}. \end{cases} \tag{9}$$

Hence, the frequency shift from the dimer bond vibration to the bulk value, $\omega(\infty) - \omega(1) \equiv -A'/(\Delta_R K_j^\kappa)$, can be obtained. The matching of the prediction with the measurement indicates that $k \equiv 1$, because $\Delta_R \propto K_j^{-1}$.

Figure 1 shows that the BOLS predictions match exceedingly well with the theoretically calculated or the experimentally measured optical redshift of a number of samples, which justifies in turn the validity of the approximation in Eq. (4) that the contribution of the high-order contribution is negligible. The derived information about the corresponding dimer vibration is given in Table I.

B. Acoustic modes and intercluster interaction

Figure 2 shows the least-squares mean-root fitting of the size-dependent LFR frequency for different nanosolids. The LFR frequency depends linearly on the inverse K_j,

$$\omega(K_j) - \omega(\infty) = \frac{-A'}{K_j}. \tag{10}$$

The zero intercept at the vertical axis, $\omega(\infty) = 0$, indicates that when the K_j approaches infinity the LFR peaks disappear, which implies that the LFR modes and their blueshifts origi-

TABLE I. Vibration frequencies of isolated dimers of various nanosolids and their redshift upon bulk formation derived from simulating the size-dependent redshift of Raman optical modes as shown in Fig. 1.

Material	d (nm)	A'	$\omega(\infty)$ (cm^{-1})	$\omega(1)$ (cm^{-1})	$\omega(\infty) - \omega(1)$ (cm^{-1})
$CdS_{0.65}Se_{0.35}$	0.286	23.9	203.4	158.8	44.6
	0.286	24.3	303	257.7	45.3
CdSe	0.294	7.76	210	195.2	14.8
CeO_2	0.22	20.89	464.5	415.1	49.4
SnO_2	0.202	14.11	638	602.4	35.6
InP	0.294	7.06	347	333.5	13.5
Si	0.2632	5.32	520.0	502.3	17.7
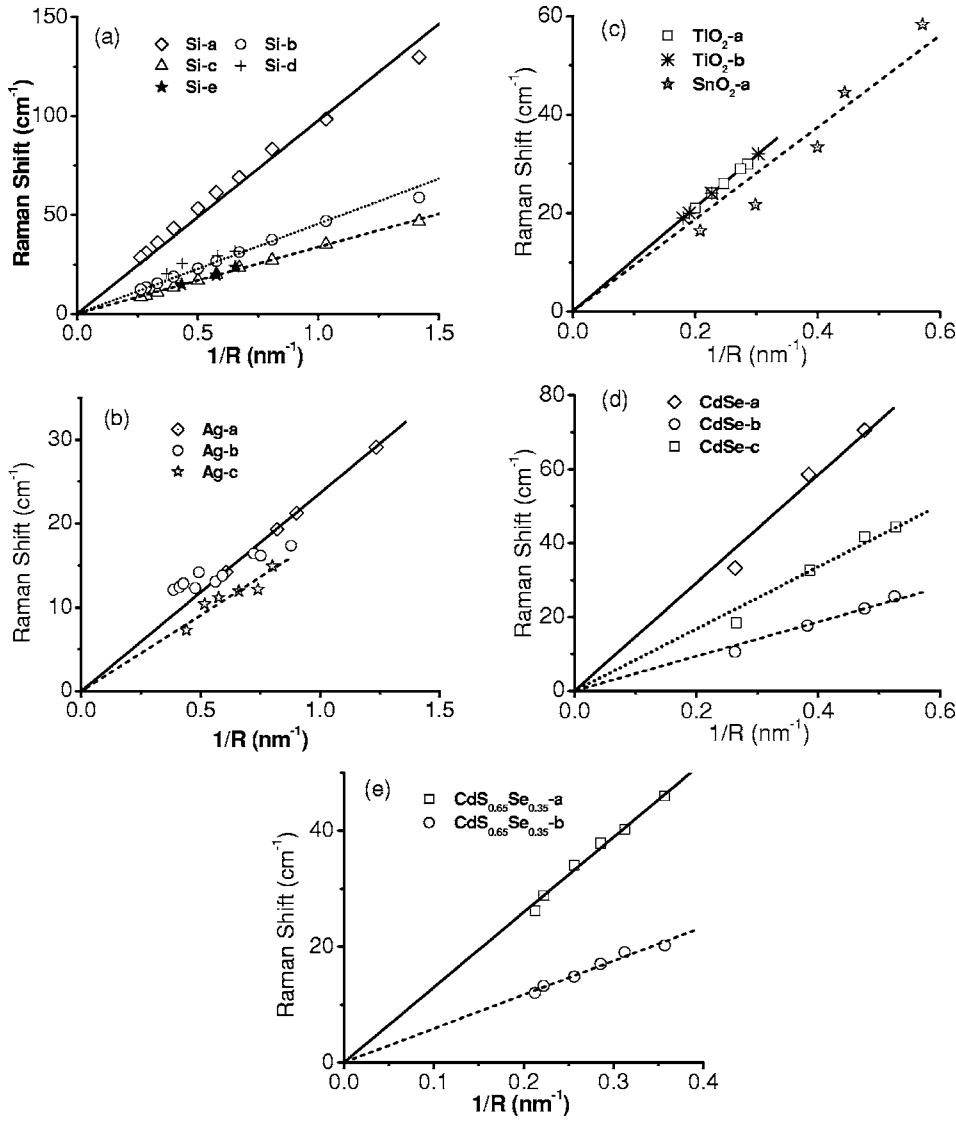
FIG. 2. Generation and blueshift of the LFR acoustic modes where the solid dotted and dashed lines are the corresponding results of the least-squares fitting. (a) The Si-*a*, Si-*b*, and Si-*c* were calculated from the lattice-dynamic matrix by using a microscopic valence force field model (Ref. 4), and the Si-*d* and Si-*e* are the experimental results (Ref. 3). (b) Ag-*a* (Ag in SiO_2) (Ref. 41), Ag-*b* (Ag in SiO_2) (Ref. 14), and Ag-*c* (Ag in alumina) (Ref. 13). (c) TiO_2-*a* (Ref. 42), TiO_2-*b* (Ref. 42), and SnO_2-*a* (Ref. 18). (d) CdSe-*a*($l=0,n=2$)   CdSe-*b*($l=2,n=1$), and CdSe-*c*($l=0,n=1$) (Ref. 43). (e) $CdS_{0.65}Se_{0.35}$-*a* [$CdS_{0.65}Se_{0.35}$ (in glass)-LF2] and $CdS_{0.65}Se_{0.35}$-*b* [$CdS_{0.65}Se_{0.35}$ (in glass)-LF1] (Ref. 37) are all measured data.

nate from vibration of the individual nanoparticle as a whole, as represented in the quadruple vibration mechanism.[13,14] It seems not essential to involve the bond strain at the interface to the LFR modes. Compared with the sophisticated lattice-dynamics calculations in which the polarized and depolarized scattering processes are considered,[11] the current derivatives treat the nanoparticle as a whole and give information about the strength of the interparticle interaction, as summarized in Table II. However, numerical agreement indicates that all models are correct though they have been established from different perspectives. The former is from the detailed process of phonon scattering while the latter is from interparticle interaction as origin.

C. Surface atom vibration

According to Einstein's relation, it can be derived that $\mu(c\omega x)^2/2z=k_BT$. At a given temperature, the vibrational amplitude and frequency of a given atom are correlated as $x \propto z^{1/2}\omega^{-1}$, which is CN dependent. The frequency and mag-

TABLE II. Linearization of the LFR acoustic modes of various nanosolids gives information about the strength of interparticle interaction for the specific solids.

Sample	A'
Ag-*a*, Ag-*b*	23.6±0.7
Ag-*c*	18.2±0.6
TiO_2-*a*, TiO_2-*b*	105.5±0.1
SnO_2-*a*	93.5±5.4
CdSe-1-*a*	146.1±6.27
CdSe-1-*b*	83.8±2.8
CdSe-1-*c*	46.7±1.4
CdSSe-*a*	129.4±1.2
CdSSe-*b*	58.4±0.8
Si-LA	97.77
Si-TA_1	45.57
Si-TA_2	33.78

nitude of vibration for an surface atom at the surface ($z=4$) or a metallic monatomic chain (MC with $z=2$) can be derived as

$$\frac{\omega_1}{\omega_b} = z_{ib} c_1^{-(m/2+1)} = \begin{cases} 0.88^{-3.44}/3 = 0.517 & (Si, m = 4.88), \\ 0.88^{-3/2}/3 = 0.404 & (metal, m = 1), \\ 0.70^{-3/2}/6 = 0.2846 & (MC, m = 1), \end{cases}$$

and

$$\frac{x_1}{x_b} = (z_1/z_b)^{1/2} \omega_b/\omega_1 = (z_b/z_1)^{1/2} c_1^{(m/2+1)}$$

$$= \begin{cases} \sqrt{3} \times 0.88^{3.44} = 1.09 & (Si), \\ \sqrt{3} \times 0.88^{3/2} = 1.43 & (metal), \quad\quad (11) \\ \sqrt{6} \times 0.70^{3/2} = 1.43 & (MC). \end{cases}$$

The vibrational amplitude of an atom at the surface or a MC is indeed greater than that of a bulk atom while the frequency is lower. The magnitude and frequency are sensitive to the m value and vary insignificantly with the curvature of a spherical dot when $K_j > 3$. This result verifies the assumption[33,34] that the vibration amplitude of a surface atom is always greater than the bulk value and it keeps constant at all particle sizes.

IV. CONCLUSION

In summary, a combination of the BOLS correlation and the scaling relation has enabled us to correlate the size-created and size-hardened LFR acoustic phonons to the intergrain interaction and the optic phonon softening to the CN-imperfection-reduced cohesive energy of atoms near the surface edge. The optic softening and acoustic hardening are realized in a K_j^{-1} fashion. Decoding the measured size dependence of the Raman optical shift we have derived vibrational information on Si, InP, CdS, CdSe, TiO_2, CeO_2, and SnO_2 dimers and their bulk shifts, which is beyond the scope of direct measurement. As the approach proceeds in a way from a bond-by-bond, atom-by-atom, shell-by-shell approach, no other constraints for the continuum medium are applied. One striking significance is that we are able to verify the correlation between the magnitude and frequency of the vibration of the lower-coordinated atoms. Consistency between the BOLS predictions and observations also verifies the validity of other possible models that incorporate the size-induced Raman shift from different perspectives. The findings gained herewith and progress made so far by practitioners gives further evidence of the impact of bond order loss and the essentiality and validity of the BOLS correlation mechanism in describing the behavior of low-dimensional systems.

*FAX: 65 6792 0415. Electronic address: ecqsun@ntu.edu.sg

[1] T. Takagahara, Phys. Rev. Lett. **71**, 3577 (1993).

[2] J. Zi, H. Büscher, C. Falter, W. Ludwig, K. M. Zhang, and X. D. Xie, Appl. Phys. Lett. **69**, 200 (1996).

[3] M. Fujii, Y. Kanzawa, S. Hayashi, and K. Yamamoto, Phys. Rev. B **54**, R8373 (1996).

[4] W. Cheng and S. F. Ren, Phys. Rev. B **65**, 205305 (2002).

[5] Y.-N. Hwang, S. Shin, H. L. Park, S.-H. Park, U. Kim, H. S. Jeong, E.-J. Shin, and D. Kim, Phys. Rev. B **54**, 15120 (1996).

[6] M. C. Klein, F. Hache, D. Ricard, and C. Flytzanis, Phys. Rev. B **42**, 11123 (1990).

[7] C. Trallero-Giner, A. Debernardi, M. Cardona, E. Menendez-Proupin, and A. I. Ekimov, Phys. Rev. B **57**, 4664 (1998).

[8] G. Viera, S. Huet, and L. Boufendi, J. Appl. Phys. **90**, 4175 (2001).

[9] P. M. Fauchet and I. H. Campell, Crit. Rev. Solid State Mater. Sci. **14**, S79 (1988).

[10] X. H. Hu and J. Zi, J. Phys.: Condens. Matter **14**, L671 (2002).

[11] J. Zi, K. Zhang, and X. Xie, Phys. Rev. B **58**, 6712 (1998).

[12] A. K. Sood, K. Jayaram, D. Victor, and S. Muthu, J. Appl. Phys. **72**, 4963 (1992).

[13] B. Palpant, H. Portales, L. Saviot, J. Lerme, B. Prevel, M. Pellarin, E. Duval, A. Perez, and M. Broyer, Phys. Rev. B **60**, 17107 (1999).

[14] M. Fujii, T. Nagareda, S. Hayashi, and K. Yamamoto, Phys. Rev. B **44**, 6243 (1991).

[15] H. Lamb, Proc. London Math. Soc. **13**, 189 (1882).

[16] G. Scamarcio, M. Lugara, and D. Manno, Phys. Rev. B **45**, 13792 (1992).

[17] L. H. Liang, C. M. Shen, X. P. Chen, W. M. Liu, and H. J. Gao, J. Phys.: Condens. Matter **16**, 267 (2004).

[18] A. Dieguez, A. Romano-Rodríguez, A. Vila, and J. R. Morante, J. Appl. Phys. **90**, 1550 (2001).

[19] Z. Iqbal and S. Vepřek, J. Phys. C **15**, 377 (1982).

[20] E. Anastassakis and E. Liarokapis, J. Appl. Phys. **62**, 3346 (1987).

[21] H. Richter, Z. P. Wang, and L. Ley, Solid State Commun. **39**, 625 (1981).

[22] I. H. Campbell and P. M. Fauchet, Solid State Commun. **58**, 739 (1986).

[23] C. Q. Sun, Prog. Mater. Sci. **48**, 521 (2003).

[24] N. Ohtani and K. Kawamura, Solid State Commun. **75**, 711 (1990).

[25] L. Banyai and S. W. Koch, *Semiconductor Quantum Dots* (World Scientific, Singapore, 1993).

[26] A. Tanaka, S. Onari, and T. Arai, Phys. Rev. B **45**, 6587 (1992).

[27] L. K. Pan, C. Q. Sun, and C. M. Li, J. Phys. Chem. B **108**, L3404 (2004).

[28] C. Q. Sun, C. M. Li, S. Li, and B. K. Tay, Phys. Rev. B **69**, 245402 (2004).

[29] C. Q. Sun, Phys. Rev. B **69**, 045105 (2004).

[30] C. Q. Sun, H. L. Bai, B. K. Tay, S. Li, and E. Y. Jiang, J. Phys. Chem. B **107**, 7544 (2003).

[31] V. M. Goldschmidt, Ber. Dtsch. Chem. Ges. B **60**, 1270 (1927); L. Pauling, J. Am. Chem. Soc. **69**, 542 (1947); P. J. Feibelman, Phys. Rev. B **53**, 13740 (1996).

[32] M. A. Omar, *Elementary Solid State Physics: Principles and Applications* (Addison-Wesley, New York, 1975), p. 403.

[33] F. G. Shi, J. Mater. Res. **91**, 307 (1994).

[34] Q. Jiang, Z. Zhang, and J. C. Li, Chem. Phys. Lett. **22**, 549 (2003).

[35] C. Ossadnik, S. Vepřek, and I. Gregora, Thin Solid Films **337**, 148 (1999).

[36] G. X. Cheng, H. Xia, K. J. Chen, W. Zhang, and X. K. Zhang, Phys. Status Solidi A **118**, K51 (1990).

[37] P. Verma, L. Gupta, S. C. Abbi, and K. P. Jain, J. Appl. Phys. **88**, 4109 (2000).

[38] J. E. Spanier, R. D. Robinson, F. Zhang, S. W. Chan, and I. P. Herman, Phys. Rev. B **64**, 245407 (2001).

[39] C. H. Shek, G. M. Lin, and J. K. L. Lai, Nanostruct. Mater. **11**, 831 (1999).

[40] M. J. Seong, O. I. Micic, A. J. Nozik, A. Mascarenhas, and H. M. Cheong, Appl. Phys. Lett. **82**, 185 (2003).

[41] P. Gangopadhyay, R. Kesavamoorthy, K. G. M. Nair, and R. Dhandapani, J. Appl. Phys. **88**, 4975 (2000).

[42] M. Gotić, M. Ivanda, A. Sekulić, S. Musić, S. Popović, A. Turković, and K. Furić, Mater. Lett. **28**, 225 (1996).

[43] L. Saviot, B. Champagnon, E. Duval, I. A. Kudriavtsev, and A. I. Ekimov, J. Non-Cryst. Solids **197**, 238 (1996).